

# The two gap transitions in $\text{Ge}_{1-x}\text{Sn}_x$ : Effect of non-substitutional complex defects

J. D. Querales-Flores, C. I. Ventura, J. D. Fuhr, and R. A. Barrio

Citation: *Journal of Applied Physics* **120**, 105705 (2016); doi: 10.1063/1.4962381


View online: <http://dx.doi.org/10.1063/1.4962381>

View Table of Contents: <http://aip.scitation.org/toc/jap/120/10>

Published by the *American Institute of Physics*

---

---



Small Conferences. BIG Ideas.

Applied Physics  
Reviews

**SAVE THE DATE!**  
**3D Bioprinting: Physical and Chemical Processes**  
May 2–3, 2017 • Winston Salem, NC, USA

# The two gap transitions in $\text{Ge}_{1-x}\text{Sn}_x$ : Effect of non-substitutional complex defects

J. D. Querales-Flores,<sup>1,2</sup> C. I. Ventura,<sup>1,3</sup> J. D. Fuhr,<sup>1,2</sup> and R. A. Barrio<sup>4</sup>

<sup>1</sup>Centro Atómico Bariloche-CNEA and CONICET, Av. Bustillo Km. 9.5, 8400 Bariloche, Argentina

<sup>2</sup>Instituto Balseiro, Univ. Nac. de Cuyo and CNEA, 8400 Bariloche, Argentina

<sup>3</sup>Univ. Nac. de Río Negro, 8400 Bariloche, Argentina

<sup>4</sup>Instituto de Física, U.N.A.M., Ap. Postal 20-364, 01000 México D.F., Mexico

(Received 15 March 2016; accepted 25 August 2016; published online 13 September 2016)

The existence of non-substitutional  $\beta$ -Sn defects in  $\text{Ge}_{1-x}\text{Sn}_x$  alloys was confirmed by emission channeling experiments [Decoster *et al.*, Phys. Rev. B **81**, 155204 (2010)], which established that, although most Sn enters substitutionally ( $\alpha$ -Sn) in the Ge lattice, a second significant fraction corresponds to the Sn-vacancy defect complex in the split-vacancy configuration ( $\beta$ -Sn), in agreement with our previous theoretical study [Ventura *et al.*, Phys. Rev. B **79**, 155202 (2009)]. Here, we present the electronic structure calculations for  $\text{Ge}_{1-x}\text{Sn}_x$ , including the substitutional  $\alpha$ -Sn as well as the non-substitutional  $\beta$ -Sn defects. To include the presence of the non-substitutional complex defects in the electronic structure calculation for this multi-orbital alloy problem, we extended the approach for the purely substitutional alloy by Jenkins and Dow [Phys. Rev. B **36**, 7994 (1987)]. We employed an effective substitutional two-site cluster equivalent to the real non-substitutional  $\beta$ -Sn defect, which was determined by a Green's functions calculation. We then calculated the electronic structure of the effective alloy purely in terms of substitutional defects, embedding the effective substitutional clusters in the lattice. Our results describe the two transitions of the fundamental gap of  $\text{Ge}_{1-x}\text{Sn}_x$  as a function of the total Sn-concentration: namely, from an indirect to a direct gap, first, and the metallization transition at a higher  $x$ . They also highlight the role of  $\beta$ -Sn in the reduction of the concentration range, which corresponds to the direct-gap phase of this alloy of interest for the optoelectronics applications. Published by AIP Publishing.

[<http://dx.doi.org/10.1063/1.4962381>]

## I. INTRODUCTION

The semiconductor technology based on Si has limitations for the optoelectronic and photovoltaic device applications, because of the indirect nature of the fundamental bandgap, which results in an inefficient absorption and emission of light. To overcome these limitations, the direct energy-gap materials based on group IV semiconductors have been searched.<sup>1-4</sup> Among group-IV elements, Ge is considered an important candidate to replace the Si in the semiconducting applications,<sup>1</sup> because it has a larger free-carrier mobility and a lower dopant activation temperature,<sup>2</sup> which makes it an attractive material in the future metal-oxide semiconductor field-effect transistors.<sup>5,6</sup> The  $\text{Ge}_{1-x}\text{Sn}_x$  alloys have attracted a considerable attention because they become direct bandgap semiconductors above  $\sim 6\%$ – $10\%$  Sn without an external mechanical strain. Moreover, the theoretical calculations indicated that strained  $\text{Ge}_{1-x}\text{Sn}_x$  ( $x < 0.17$ ) would exhibit an enhanced electron and hole mobility, which could make the alloy also interesting for the high-speed integrated circuits.<sup>8,9</sup> The integration of Ge in the Si-based photonics is important for advances in the performance of detectors, modulators, and emitters.

Experimental studies in the group-IV alloys were hindered for a long time by the sample preparation problems. When the  $\text{Ge}_{1-x}\text{Sn}_x$  samples are experimentally prepared, the distribution of the Sn atoms in the Ge matrix depends on the growth conditions: The Sn-atoms can enter randomly,<sup>10</sup> form a regular superstructure,<sup>11</sup> or coalesce into a larger

cluster.<sup>1,10,12</sup> At a temperature below  $13^\circ\text{C}$ , pure Sn exists in the  $\alpha$ -Sn (gray tin) phase with a diamond structure, but it undergoes a phase transition to  $\beta$ -Sn (white-tin) above this temperature.<sup>13</sup> Experiments have shown that a problem with the incorporation of the Sn into the Ge lattice is the large  $\sim 17\%$  lattice mismatch between these elements and the instability of the diamond-cubic structure of the  $\alpha$ -Sn above  $13^\circ\text{C}$ .<sup>4,14</sup> Although the  $\text{Ge}_{1-x}\text{Sn}_x$  alloys have been successfully grown by molecular beam epitaxy,<sup>15</sup> chemical vapor deposition,<sup>4</sup> and enhanced direct bandgap luminescence that has been demonstrated for up to  $8\%$  Sn,<sup>16,17</sup> at higher Sn-concentrations, several limitations arise due to the low thermodynamic solid solubility of Sn in the Ge crystal, which is less than  $1\%$ , and, in many cases, the material quality is questionable due to the propensity of Sn to segregate toward the film surface.<sup>4,14,18</sup> Recently, the fabrication of a high quality  $\text{Ge}_{1-x}\text{Sn}_x$  on InGaAs buffer layers using a low-temperature growth by the molecular beam epitaxy was reported.<sup>15</sup> X-ray diffraction, secondary ion mass spectroscopy, and transmission electron microscopy studies demonstrated that up to  $10.5\%$  Sn had been incorporated into the  $\text{Ge}_{1-x}\text{Sn}_x$  thin films without Sn precipitation.<sup>15</sup> More recently, the  $\text{Ge}_{1-x}\text{Sn}_x$  homogeneous epitaxial layers were grown on the InP substrates for the range  $0.15 < x < 0.27$ .<sup>12</sup> The direct bandgap for the Sn-concentration range  $0.15 < x < 0.27$  was obtained through the photon absorption spectra measured with the Fourier transform infrared spectroscopy.

The incorporation of Sn in the Ge matrix has been investigated theoretically by Ventura *et al.*<sup>19,20</sup> Through local defect electronic calculations, the formation of several complex Sn-defects in the  $\text{Ge}_{1-x}\text{Sn}_x$  alloy was analyzed, confirming that, at low Sn concentrations, substitutional  $\alpha$ -Sn, in which a Sn atom occupies the position of a Ge atom in the diamond lattice, is favoured. Above a certain critical Sn concentration<sup>19,20</sup> dependent on temperature, Sn could also appear as the non-substitutional  $\beta$ -Sn complex defect, in which an interstitial Sn-atom occupies the center of a divacancy in the Ge lattice. The metallic Sn clusters resulting in inhomogeneous defect structures could appear at still higher Sn concentrations.<sup>20</sup> In 2010, emission channeling experiments by Decoster *et al.*<sup>21</sup> confirmed the existence of the  $\beta$ -Sn defects in the homogeneous  $\text{Ge}_{1-x}\text{Sn}_x$  alloy, establishing that they represented the second significant fraction of Sn incorporated in the Ge lattice, most Sn atoms entering substitutionally ( $\alpha$ -Sn) in Ge. The existence of such a defect in the amorphous Ge-Sn alloys had already been confirmed by detailed Mössbauer experiments,<sup>22</sup> which in fact showed a signal corresponding to a Sn atom in an octahedral environment, besides the expected signal of the tetrahedral environment corresponding to the substitutional  $\alpha$ -Sn. The local environment and the interactions of  $\alpha$ -Sn, the Ge vacancy and  $\beta$ -Sn, confirming that  $\beta$ -Sn could be formed by the natural diffusion of a vacancy around  $\alpha$ -Sn because of the small energy barrier for the process, have been also studied.<sup>23</sup>

The tunability of its gap with the composition makes  $\text{Ge}_{1-x}\text{Sn}_x$  a highly interesting material for the infrared applications, especially at low Sn concentrations ( $x < 0.20$ ).<sup>7</sup> The  $\text{Ge}_{1-x}\text{Sn}_x$  alloys with high Sn concentrations could also be important as an alternative to the HgCdTe system for the far-infrared applications, as the II-VI compounds are expensive and incompatible with the Si technologies.<sup>24</sup> Recently, there have been reports of a room temperature direct bandgap emission for the Si-substrate-based Ge p-i-n heterojunction photodiode structures, operated under forward bias.<sup>25</sup> A temperature-dependent photoluminescence (PL) study has been conducted<sup>26</sup> in the  $\text{Ge}_{1-x}\text{Sn}_x$  films with Sn compositions of 0.9%, 3.2%, and 6.0% grown on Si. The competition between the direct and indirect bandgap transitions was clearly observed. The relative peak intensity of the direct transition with respect to the indirect transition increases with an increase in temperature, indicating that the direct transition dominates the PL at high temperatures. Furthermore, as the Sn composition increases, a progressive enhancement of the PL intensity corresponding to the direct transition was observed,<sup>26</sup> due to the reduction of the direct-indirect valley separation, which experimentally confirms that the  $\text{Ge}_{1-x}\text{Sn}_x$  grown on Si becomes a group IV-based direct bandgap material by increasing the Sn content. More recently, the fabrication and properties of the  $\text{Ge}_{1-x}\text{Sn}_x$  ( $x < 0.123$ ) *pn* diodes were reported.<sup>27</sup> Electroluminescence results indicated that the emission properties depend very sensitively on the Sn-concentrations on both sides of the junctions, making this system not only a serious candidate for laser devices but also an ideal model system to study the properties of the quasi-direct light emitting devices.

Experimentally, a series of values have been reported for the critical Sn concentration for the indirect to direct gap transition, hereafter denoted  $x_c^I$ : starting from Ref. 7 whose optical absorption experiments predicted  $0.11 < x_c^I < 0.15$ , followed by Ladrón de Guevara *et al.*<sup>28</sup> who reported  $0.10 < x_c^I < 0.13$  from transmittance measurements, D'Costa *et al.*<sup>4</sup> who reported  $x_c^I \sim 0.11$  with ellipsometry experiments, and, more recently, Chen *et al.*<sup>16</sup> reported  $x_c^I \sim 0.07$  using photoluminescence. Then,  $x_c^I \sim 0.06 - 0.08$  was suggested, based on the photoluminescence studies of the strain free-GeSn layers.<sup>16,17</sup> Ryu *et al.*,<sup>29</sup> by means of temperature-dependent photoluminescence experiments of Ge/Si and  $\text{Ge}_{1-y}\text{Sn}_y/\text{Si}$ , indicated a possible indirect-to-direct bandgap transition at the Sn content  $\sim 0.06$ , consistent with the density functional theory (DFT) calculations in Ref. 30. More recently, by a fit to experimental data in  $\text{Ge}_{1-x}\text{Sn}_x$  using a theoretical model of the bandgap bowing, Gallagher *et al.*<sup>31</sup> estimated a cross-over concentration of  $x_c^I = 0.09$ , significantly increased from earlier estimations based on a strictly quadratic compositional dependence of the bandgaps in Ref. 32, who obtained  $x_c^I = 0.073$ .

In this work, we concentrated on the electronic structure calculations for  $\text{Ge}_{1-x}\text{Sn}_x$ , including the substitutional  $\alpha$ -Sn as well as the non-substitutional  $\beta$ -Sn defects. At present, the *ab-initio* electronic structure calculations include individual non-substitutional defects, such as interstitials, but no standard approaches are available to calculate the band structure of alloys involving the non-substitutional complex defects formed by many components. An example of such complex defects would be an interstitial impurity atom attached to a divacancy, as is the case for the “ $\beta$ -Sn” defects in Ge. In order to take into account the non-substitutional complex defects in the electronic structure calculation for this multi-orbital alloy problem, we transformed the real alloy problem into an equivalent purely substitutional effective alloy problem. For this, we employed an effective substitutional two-site cluster equivalent to the real non-substitutional  $\beta$ -Sn defect and extended the approach originally proposed by Jenkins and Dow<sup>33</sup> for the purely substitutional alloy, who used 20 tight-binding (TB)  $sp^3s^*$  orbitals for the group IV elements combined with the virtual crystal approximation (VCA) for the substitutional disorder.

This paper is organized as follows. We present in Sec. II a brief description of our proposal for the inclusion of the  $\beta$ -Sn non-substitutional defects in the electronic structure calculation. In Sec. II B 1, we discuss the indirect-to-direct gap transition in  $\text{Ge}_{1-x}\text{Sn}_x$ , as described by our present extension of the TB + VCA approach, adjusted to experimental data. In the Appendix, we show how the present TB + VCA approach allows to improve the theoretical description of experimental direct gap results for the substitutional  $\text{Ge}_{1-x-y}\text{Si}_x\text{Sn}_y$  ternary alloys. The results of our present electronic structure calculation for binary  $\text{Ge}_{1-x}\text{Sn}_x$  with the present approach, including the non-substitutional  $\beta$ -Sn as well as the substitutional  $\alpha$ -Sn, are presented in Sec. III. In Sec. IV, we summarize the conclusions of our work.

## II. INCLUSION OF THE $\beta$ -Sn NON-SUBSTITUTIONAL COMPLEX DEFECTS IN THE ELECTRONIC STRUCTURE CALCULATION

Above a critical Sn concentration, the non-substitutional  $\beta$ -Sn defects become important,<sup>20,21</sup> but there are currently no electronic structure approaches that include their effect. To fill this important gap, we devised an analytical method that makes it possible to incorporate the  $\beta$ -Sn defects within the framework of the virtual crystal approximation. A first implementation was presented in Ref. 38, although the present proposed method includes improvements allowing us to refine our description of  $\text{Ge}_{1-x}\text{Sn}_x$ . VCA assumes a random alloy to be composed of “virtual” atoms, forming a periodic crystal potential modelled as a composition-weighted average of the constituent element potentials. To include  $\beta$ -Sn in the electronic structure calculation, we extend the TB + VCA approach by Jenkins and Dow<sup>33</sup> for the substitutional  $\text{Ge}_{1-x}\text{Sn}_x$  alloy. In the latter, only a substitutional  $\alpha$ -Sn was assumed to be present, and a 20-orbital TB basis ( $s, p, s^*$  states) was introduced for group IV elements. The  $20 \times 20$  Jenkins-Dow tight-binding Hamiltonian includes: the second-neighbor<sup>33,34</sup> and spin-orbit interactions.<sup>33,35–37</sup>

For our present electronic structure calculation, we started by considering the  $\text{Ge}_{1-x}\text{Sn}_x$  alloy formed by three components: Ge,  $\alpha$ -Sn, and  $\beta$ -Sn atoms, as an effective binary alloy composed by two components: one, represented by the (Ge +  $\alpha$ -Sn) substitutional alloy as considered by Jenkins and Dow,<sup>33</sup> and the other component represented the  $\beta$ -Sn non-substitutional defects. For the latter, we proposed an effective substitutional 2-site cluster equivalent to the real non-substitutional  $\beta$ -Sn,<sup>38</sup> as illustrated in Fig. 1 and detailed in Subsection II A. In Subsection II B, we present our extension of the Jenkins-Dow TB + VCA calculation to treat the effective substitutional binary alloy representing the real alloy with Ge,  $\alpha$ -Sn and  $\beta$ -Sn.

### A. Effective substitutional two-site cluster equivalent to the non-substitutional $\beta$ -Sn defect

As mentioned earlier, in a previous work,<sup>38</sup> we determined and compared two effective substitutional two-site clusters equivalent to the real non-substitutional  $\beta$ -Sn defects, which is schematically represented in Fig. 1. In Fig. 1(a), we depict the real non-substitutional  $\beta$ -Sn defect (with energy  $E_{\beta\text{-Sn}}^\gamma$ , where  $\gamma$  represents each basis orbital ( $\gamma = s, p, s^*$ ) in its six fold coordinated configuration). Meanwhile, Fig. 1(b) represents an equivalent cluster composed by two substitutional sites, where the effective atoms occupying each site in the cluster have an energy denoted by  $E_1^\gamma$  (considered to be equal in both sites of the cluster, by symmetry).<sup>38</sup>

The equivalence was established under the following conditions: (1) for simplicity, we proposed that the equivalence was valid for each separate orbital; (2) we assumed that only interactions between orbitals of the same type between the nearest-neighbour (NN) atoms are relevant; and (3) we demanded that the local Green's functions in the original and equivalent problem be equal and will thus have the same analytical properties.

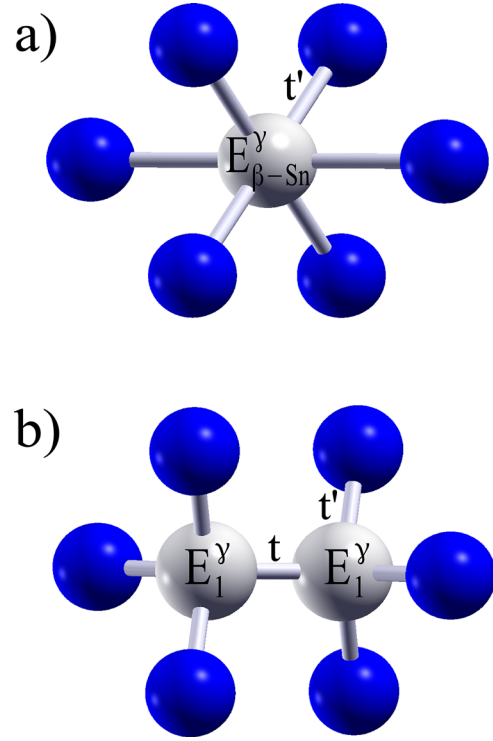


FIG. 1. (a) Non-substitutional  $\beta$ -Sn, (b) substitutional 2-site cluster equivalent for  $\beta$ -Sn. Blue balls: Ge atoms (lattice with diamond symmetry); gray balls: Sn atoms, (a): The Sn-atom located at the center of a Ge-divacancy and (b): The Sn-atoms in substitutional positions.  $t'$  represents a hopping between a Sn-atom and the nearest neighbors Ge-atoms.  $t$  denoted an intra-cluster hopping between Sn atoms on substitutional representation.

Due to our investigation in Ref. 38, no qualitative differences are expected for the electronic structure obtained using equivalent clusters with a null intra-cluster hopping  $t=0$  or with an intra-cluster hopping equal to that between the cluster and the rest of the lattice:  $t=t'$ .

Thus, in our present work, we adopted the effective equivalent substitutional cluster with  $t=0$ , to represent the  $\beta$ -Sn non-substitutional defects. In this case, from Ref. 38 we have

$$E_1^\gamma \simeq (E_{\beta\text{-Sn}}^\gamma + t'). \quad (1)$$

The energy of the effective pseudo-atoms with the correct symmetry has been expressed in terms of energy parameters corresponding to the original  $\beta$ -Sn defect, allowing the incorporation of these non-substitutional defects in the electronic structure calculation of the alloy under study in terms of the substitutional defects.

### B. TB + VCA extension to include $\alpha$ -Sn and non-substitutional $\beta$ -Sn in the $\text{Ge}_{1-x}\text{Sn}_x$ electronic structure calculation

To obtain the virtual-crystal band structure of  $\text{Ge}_{1-x}\text{Sn}_x$ , including the substitutional  $\alpha$ -Sn and non-substitutional  $\beta$ -Sn, we proposed the following extension for the TB + VCA approximation of the substitutional alloy originally proposed by Jenkins and Dow.<sup>33</sup> We used the same basis of 20 tight-binding orbitals (with  $s, p, s^*$  character) introduced by Jenkins and Dow for group IV elements, but in the diagonal part of



the Hamiltonian, we added a set of three orbital weight factors, depending on the orbital character of the basis state, and took into account the presence of  $\beta$ -Sn. Concretely, we considered the following matrix elements for the TB + VCA Hamiltonian of the binary alloy:

$$\begin{aligned}\mathcal{H}_{ii}^\gamma &= (1-x)[Ge]_{ii}^\gamma + W_\gamma \left( x_\alpha [\alpha-Sn]_{ii}^\gamma + x_\beta [\beta-Sn]_{ii}^\gamma \right); \\ \mathcal{H}_{ij}^\gamma &= \frac{\left[ (1-x)[Ge]_{ij}^\gamma \{a_{Ge}\}^2 + x[\alpha-Sn]_{ij}^\gamma \{a_{Sn}\}^2 \right]}{\{a(x)\}^2},\end{aligned}\quad (2)$$

where  $\mathcal{H}_{ii}^\gamma$  and  $\mathcal{H}_{ij}^\gamma$  denote the diagonal and non-diagonal matrix elements of the Hamiltonian, respectively, the subindices  $i$  and  $j$  refer to the TB-orbital states, and  $\gamma$  denotes each Hamiltonian block with  $s$ ,  $p$ , or  $s^*$  orbital character. Further details of the structure of this TB Hamiltonian can be found in Ref. 33. By  $[Ge]$  and  $[\alpha-Sn]$  we refer to the tight-binding parameters for pure Ge or for  $\alpha$ -Sn, respectively, as given in Ref. 33. Meanwhile,  $[\beta-Sn]$  denotes the TB Hamiltonian matrix elements corresponding to the substitutional equivalent used for the real non-substitutional defect, in our case:  $[\beta-Sn] = E_1^\gamma = [\beta-Sn] + t'$ . In our present calculations, for simplicity, we have assumed that a Sn-atom has the same tight-binding parameters in both the configurations:  $\alpha$ -Sn and  $\beta$ -Sn. By  $x_\alpha$  and  $x_\beta$ , we denote the relative concentration of  $\alpha$ -Sn and  $\beta$ -Sn, respectively, in  $Ge_{1-x}Sn_x$ ; therefore,  $x = x_\alpha + x_\beta$ .

In the diagonal matrix elements of the Hamiltonian above, we introduced three orbital weight factors:  $W_\gamma$  ( $\gamma = s$ ,  $s^*$  or  $p$ ), in order to reproduce as closely as possible the band structure of  $Ge_{1-x}Sn_x$  alloys, according to recent experiments,<sup>4,7,31</sup> and, in particular, to improve the description of the indirect to direct gap transition of the substitutional alloy with respect to the original approach by Jenkins and Dow.<sup>33</sup>  $W_\gamma$  were included as factors of the Sn-atoms contribution to the diagonal matrix elements, as the pure Ge indirect (and direct) gaps<sup>49</sup> are correctly described by the Jenkins and Dow TB elements.<sup>33</sup> In Sec. II B 1, we will discuss in detail the parametrization adopted for these  $W_\gamma$  parameters.

It has to be noted that we had adopted the non-diagonal Hamiltonian matrix elements of Jenkins and Dow,<sup>33</sup> which include the lattice parameters for Ge and  $\alpha$ -Sn, namely:  $a_{Ge} = 5.65$  Å, and  $a_{Sn} = 6.46$  Å, and we assumed that Vegard's law<sup>39</sup> is valid for the binary alloy lattice parameter, thus:  $a(x) = (1-x)a_{Ge} + xa_{Sn}$ .

The present extension of TB + VCA enables us to tackle two important issues in  $Ge_{1-x}Sn_x$ : (1) as already mentioned, a more realistic description of the crossover from an indirect to a direct fundamental bandgap, according to recent experiments, and (2) the inclusion of the non-substitutional complex  $\beta$ -Sn defects in the electronic structure calculation, which has been confirmed to exist by experiments, and as we will show would play an important role in the electronic properties of the  $Ge_{1-x}Sn_x$ , basically limiting the direct gap phase of interest for the optoelectronics applications.

### 1. The parametrization of $W_\gamma$ : Indirect to direct gap transition in substitutional $Ge_{1-x}Sn_x$

Next, we have explained how we optimized the values of the weight parameters:  $W_\gamma$  ( $\gamma = s$ ,  $s^*$  or  $p$ ), introduced in

Eq. (2), in order to properly reproduce the available experimental data of  $Ge_{1-x}Sn_x$  alloys, and in particular, the critical Sn-concentration  $x_c^I$  for the indirect to direct gap transition in the substitutional  $Ge_{1-x}Sn_x$ .

Using the original TB + VCA approach for substitutional  $Ge_{1-x}Sn_x$  by Jenkins and Dow,<sup>33</sup> one obtains  $x_{c-ID}^I = 0.15$ .<sup>20</sup> Recently, other theoretical predictions were reported:  $x_c^I = 0.17$  was obtained with a charge self-consistent pseudopotential plane wave method,<sup>40</sup>  $x_c^I = 0.11$  with the empirical pseudopotential method with adjustable form factors fitted to experimental data,<sup>41</sup> while the full potential augmented plane wave plus local orbital method within the density functional theory (DFT) yielded:  $x_c^I = 0.105$ .<sup>42</sup> Gupta *et al.*<sup>43</sup> predicted  $x_c^I = 0.065$ , using a theoretical model based on the nonlocal empirical pseudopotential method. Eckhardt *et al.*,<sup>44</sup> predicted  $x_c^I \sim 0.1$  for the  $Ge_{1-x}Sn_x$  grown commensurately on Ge(100) substrates, using a supercell approach and VCA, with DFT in the local density approximation.

Our extension of the TB + VCA described in Subsection II B includes three orbital weight parameters  $W_\gamma$  ( $\gamma = s$ ,  $s^*$  or  $p$ ), which we introduced to improve the fit of the TB model to experimental electronic structure results. They enable us to construct a TB model to correctly reproduce the experimental data reported for the indirect and direct bandgaps of Ge and  $Ge_{1-x}Sn_x$  at particular alloy concentrations.<sup>4,7,16,31</sup> In our present work, we adjusted  $W_\gamma$  ( $\gamma = s$ ,  $s^*$  or  $p$ ), using experimental data for the indirect and direct bandgaps of pure Ge ( $x=0$ ) and  $Ge_{0.85}Sn_{0.15}$ : obtained by He and Atwater<sup>7</sup> through optical absorption experiments, later confirmed by transmittance measurements by D'Costa *et al.*<sup>4</sup> and by the recent room-temperature photoluminescence spectroscopy data by Gallagher *et al.*<sup>31</sup> The set of optimal weight factors obtained by fitting these data are

$$W_s = 1.256, \quad W_{s^*} = 1.020, \quad W_p = 1.00. \quad (3)$$

Regarding the choice of the weight factors specified in Equation (4), it was done taking into account our study of the orbital character of the eigenvectors along the Brillouin zone (BZ),<sup>38</sup> and, in particular, at the symmetry points, which define the fundamental bandgap, depending on the alloy composition: namely, the BZ center,  $\Gamma$ , with the relevant valence band maximum, the conduction band minimum determining the direct gap, and the BZ point  $L = (2\pi/a(x))(1/2, 1/2, 1/2)$ , which corresponds to the location of the conduction band minimum that determines the indirect gap in Ge. At  $\Gamma$ , we find that the eigenvectors correspond mainly to  $s$ -states at the conduction band minimum and mainly  $p$ -states at the valence band maximum, while at  $L$ , the eigenvectors correspond mostly to  $(s + s^*)$ -states, although a minor proportion of  $p$ -character is retained, and these results do not exhibit significant changes increasing the Sn-concentration. Meanwhile, increasing  $x$  the energy of the valence band maximum at  $\Gamma$  remains almost fixed, while it is the energies of the conduction band minima at  $L$ - and  $\Gamma$ , which are changed.<sup>38</sup> On the basis of these facts, we set  $W_p = 1.00$  and proceeded to adjust  $W_s$  and  $W_{s^*}$  to fit the experimental direct and indirect bandgaps<sup>4,7,16</sup> at  $x = 0.15$ .

Henceforward, the set of values for  $W_\gamma$  specified in Eq. (3) will be kept constant for all the electronic structure

calculations in this work. It can be noted that the only change to the matrix elements of the tight-binding Hamiltonian of Jenkins and Dow,<sup>33</sup> due to the introduction of these optimized weight factors  $W_\gamma$  in Eq. (2), appears in the diagonal TB parameters for  $\alpha$ -Sn (and  $\beta$ -Sn in our approximation), here given by:  $E_s = -7.3853$  eV and  $E_{s^*} = 6.0180$  eV.

In Table I, we show a comparison between the direct and indirect bandgaps obtained with the TB + VCA approach described earlier and the experimental results reported in Ref. 7 for them. As expected, there is an agreement for  $x=0$  and  $x=0.15$ , used for our fits, but at intermediate Sn concentrations, the calculated values show some deviations from the experimental ones, as discussed in Sec. III A.

A considerable improvement is obtained for the predicted critical Sn-concentration for the transition from an indirect to a direct fundamental gap in  $\text{Ge}_{1-x}\text{Sn}_x$ , which the present approach places in the vicinity of  $x_c^I = 0.088$  (with the optimized  $W_\gamma$  values, specified in Eq. (3)). This is much closer to the recently reported experimental values detailed in the Introduction than the prediction of  $x_{c-JD}^I \sim 0.15$ , obtained<sup>20</sup> using the original TB + VCA by Jenkins and Dow.<sup>33</sup> It can be noted that the simple parametrization scheme here proposed to improve the description of the experimental data of the substitutional alloy has the advantage that it can be easily adjusted to fit data placing the indirect to direct transition of the substitutional alloy at other values. The flexibility provided by this parametrization in terms of three adjustable weight parameters is especially convenient if one considers the spread of the experimental values reported for  $x_c^I$  (as mentioned in our Introduction), possibly due to the sample preparation differences.

Finally, before discussing in detail the results obtained with our approach in Sec. III, we would like to comment on two recent parametrizations of the tight binding parameters<sup>46,47</sup> and compare them with those including the spin orbit interaction and up to the second-nearest neighbour effects proposed by Jenkins and Dow.<sup>33</sup>

Küfner *et al.*,<sup>46</sup> studied the structural and electronic properties of pure  $\alpha$ -Sn nanocrystals from the first principles, using DFT within approximations based on the hybrid exchange-correlation functional and including spin-orbit interaction effects. They reported a list of the first-NN tight-binding parameters for  $\alpha$ -Sn with some differences with respect to those of Refs. 33 and 48. Replacing in the TB + VCA approach by Jenkins and Dow,<sup>33</sup> the first-NN tight-binding parameters of pure  $\alpha$ -Sn by those of Küfner *et al.*,<sup>46</sup> we find that the prediction for the indirect to direct gap transition in  $\text{Ge}_{1-x}\text{Sn}_x$  would be shifted from  $x_{c-JD}^I \sim 0.15$ <sup>20,33</sup> to  $x_c^I \sim 0.10$ .

TABLE I. A comparison between the theoretical bandgap energies in the present work and the reported experimental data of Atwater *et al.*<sup>7</sup> for  $\text{Ge}_{1-x}\text{Sn}_x$ .  $E_0$ : Direct gap and  $E_I$ : indirect gap.

$x$	$E_0$ : Exp.	$E_0$ : Theory	$E_I$ : Exp.	$E_I$ : Theory
0.00	$0.800 \pm 0.004$	0.803	$0.670 \pm 0.019$	0.670
0.06	$0.614 \pm 0.004$	0.613	$0.599 \pm 0.019$	0.578
0.11	$0.445 \pm 0.003$	0.468	$0.428 \pm 0.019$	0.502
0.15	$0.346 \pm 0.003$	0.346	$0.441 \pm 0.004$	0.441

In 2014, based on the first-NN tight-binding parameters for pure Ge of Vogl *et al.*<sup>48</sup> and those by Küfner *et al.* for  $\alpha$ -Sn,<sup>46</sup> Attiaoui and Moutanabbir<sup>47</sup> presented a semi-empirical second-NN tight-binding calculation of the electronic structure of  $\text{Ge}_{1-x-y}\text{Si}_x\text{Sn}_y$  ternary alloys as well as  $\text{Ge}_{1-x}\text{Sn}_x$ . Using the same 20 basis states as in Refs. 33, 46, and 48, they evaluated new TB parameters for the alloy components, with some changes to the previous ones also including the second-neighbours and spin orbit corrections.<sup>33</sup> For the indirect to direct gap transition in the substitutional unstrained  $\text{Ge}_{1-x}\text{Sn}_x$ , they obtain  $x_c^I \sim 0.11$ , which is smaller than  $x_{c-JD}^I \sim 0.15$  and agrees with the experimental data of Ref. 4, although it overestimates more recent experimental values mentioned in the Introduction.<sup>16,17,31</sup> Concerning the electronic structure study of the substitutional unstrained  $\text{Ge}_{1-x-y}\text{Si}_x\text{Sn}_y$  ternary alloys, the prediction of Ref. 47 is consistent with the previous results<sup>58</sup> obtained using an extension of the TB + VCA by Jenkins and Dow.<sup>33</sup> In particular, almost equal critical concentration values (with minor differences possibly related to the use of different pure Sn-lattice parameter values<sup>47,58</sup>) are predicted for the transition of the indirect gap: between two different relevant conduction band minima defining the gap (one Ge-like at Brillouin zone point L, and the other Si-like). The [supplementary material](#) can also be viewed for a comparison of the bandstructure of a pure  $\alpha$ -Sn and the ideal substitutional alloy at  $x = 0.15, 0.30$ , employing different parametrizations.

### III. RESULTS AND DISCUSSION

Here, we will present electronic structure results obtained using our approach described in Sec. II, divided in two Secs. III A and III B, respectively. In Sec. III A, we will discuss and compare in detail with recent experiments our results for the low Sn-concentration regime: where only substitutional  $\alpha$ -Sn is expected to be present. In Sec. III B, we show our predictions for  $\text{Ge}_{1-x}\text{Sn}_x$  alloys at higher Sn-concentrations where, above a temperature-dependent critical Sn-concentration, the non-substitutional  $\beta$ -Sn defects are also expected to be present.<sup>19,20</sup> In particular, for each of these two regimes, we discuss the fundamental gap transition of  $\text{Ge}_{1-x}\text{Sn}_x$  that is expected to take place.

#### A. Substitutional alloy: Results of the present approach for Ge + $\alpha$ -Sn

Using the TB + VCA approach described in Sec. II for the  $\text{Ge}_{1-x}\text{Sn}_x$  alloys in the low  $x$  regime, where all Sn atoms occupy the substitutional positions in the Ge lattice, we obtained the results exhibited in Fig. 2. There, we show the compositional dependence of the direct ( $E_0$ ) and indirect ( $E_I$ ) bandgaps of  $\text{Ge}_{1-x}\text{Sn}_x$  obtained with the present approach, intersecting at  $x_c^I = 0.088$  where the indirect to direct transition of the fundamental gap is thus predicted. For comparison, we included a series of recently available experimental data<sup>4,7,15,16,28,31,53,54</sup> and showed the indirect to direct gap transition prediction of  $x_{c-JD}^I = 0.15$ , obtained using the original TB + VCA approach,<sup>20,33</sup> which yielded a gap value of 0.568 eV at that Sn-concentration, much higher than the observed fundamental direct gap of 0.346 eV (Ref. 7) detailed in Table I.

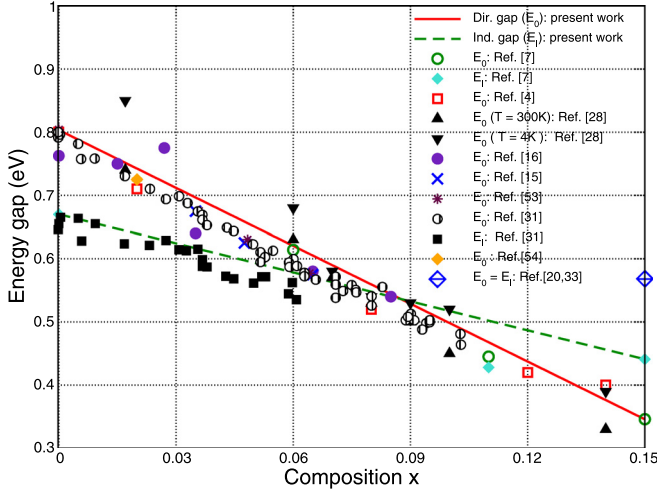


FIG. 2. A comparison between our theoretical bandgap energies (direct gap: full line, indirect gap: dashed line) yielding:  $x_c^I = 0.088$ , and available experimental data (symbols: see references in the plot), for the various Sn compositions. The theoretical gap prediction at critical  $x_{c-ID} = 0.15$  obtained<sup>20</sup> with the original TB+VCA approach<sup>33</sup> is also shown (large diamond).

The direct and indirect bandgaps obtained with our approach (in eV) can be, correspondingly, fitted as follows:

$$\begin{aligned} E_0(x) &= 0.803 - 3.047x; \\ E_I(x) &= 0.670 - 1.527x. \end{aligned} \quad (4)$$

By comparing our results with the experimental data in Fig. 2, one can notice that a relatively good description of the compositional dependence of the direct and indirect gaps was obtained, indeed much better than if a linear interpolation between the respective gap values for pure Ge and  $\alpha$ -Sn was used.<sup>4,7,16</sup> Nevertheless, small deviations from linearity in the data were evident,<sup>4,7,45</sup> as experimentally reported for the lattice constant of  $\text{Ge}_{1-x}\text{Sn}_x$  as well.<sup>45</sup> Many other binary semiconducting alloys  $\text{A}_x\text{B}_{1-x}$  also exhibited similar non-linear dependences of their physical properties as a function of alloy composition, behaviour known as *bowing effects*. Although VCA cannot describe the non-linear bowing effects, it, nevertheless, often yields good qualitative results.<sup>4</sup>

Fig. 3(a) shows the total density of states (TDOS) obtained for  $\text{Ge}_{1-x}\text{Sn}_x$  as a function of energy, at the substitutional-Sn concentrations:  $x = 0.0, 0.15, 0.25, 0.30$ . In agreement with the results obtained using the *ab-initio* FPLO5+CPA code<sup>50</sup> in Ref. 20, it can be noticed that a smooth behaviour as function of Sn concentration is obtained, with changes in the bandwidth and a progressive reduction of the gap around the  $\omega = 0$  with Sn concentration. Experiments in  $\text{Ge}_{1-x}\text{Sn}_x$ <sup>4,7,16,28,53</sup> confirmed that the direct gap decreases primarily through a Sn-content increase in the alloy.<sup>1,4,7</sup>

In Fig. 3(b), we show the total and the three partial densities of states as a function of energy for  $\text{Ge}_{0.78}\text{Sn}_{0.22}$  substitutional alloy. Around the bandgap, two peaks are visible in the density of states: the peak located just below the gap is clearly dominated by *p* orbital contributions, while *p*, *s*, and *s\** orbitals contribute to the peak located just above the gap. Moreover, we can see that the lowest band ( $\sim -12$  eV)

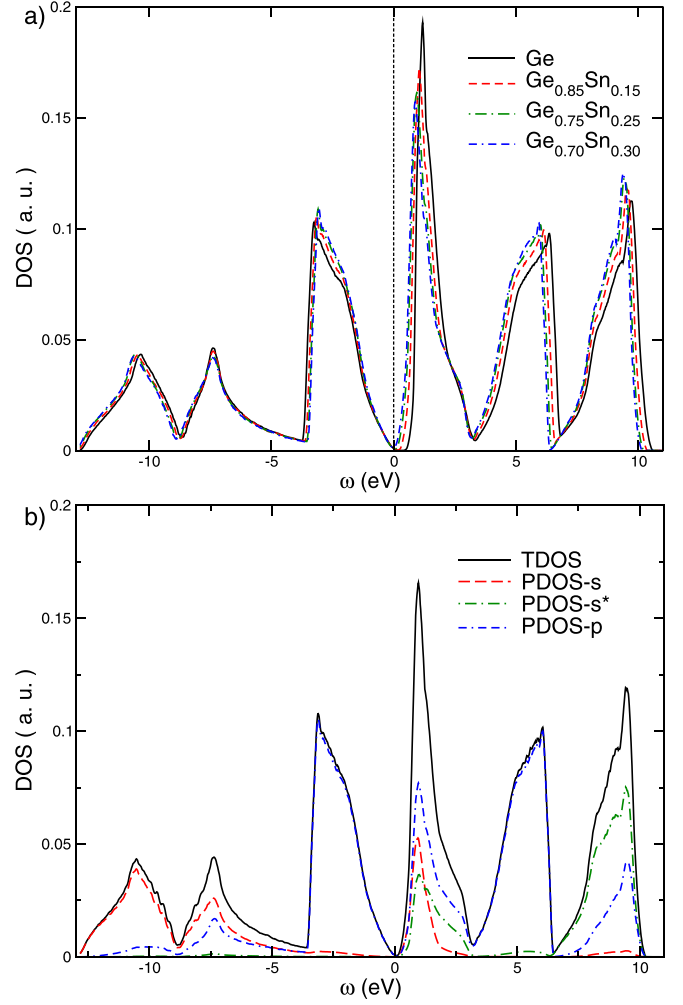


FIG. 3. Substitutional  $\text{Ge}_{1-x}\text{Sn}_x$  - results of the present TB+VCA: (a) The total density of states for the  $\alpha$ -Sn concentrations indicated in the plot; (b) the total DOS (TDOS) and partial DOS (PDOS) “*p*,” “*s*” and “*s\**” densities of states at  $x = 0.22$  ( $>x_c^I = 0.088$ ), a direct gap alloy.  $t' = -3$  eV as in Refs. 51 and 52.

corresponds essentially to *s* orbitals, while the highest band ( $\sim 10$  eV) is originated essentially by *s\** and *p* orbitals, as in pure Ge. These features also agree with the FPLO5+CPA results.<sup>20,50</sup>

In Fig. 4, we show that the band structure obtained for the substitutional  $\text{Ge}_{0.78}\text{Sn}_{0.22}$  alloy. In order to analyze the fundamental bandgap in  $\text{Ge}_{1-x}\text{Sn}_x$ , we focus on three specific BZ points that define it: the maximum of the valence band at  $\Gamma$ , the minima of the conduction band at  $\Gamma$  and at  $L$ , with energies denoted  $\Gamma_0$ ,  $\Gamma_1$ , and  $L_1$ , respectively. It can be noticed that  $\text{Ge}_{0.78}\text{Sn}_{0.22}$  possesses a fundamental direct gap:  $0.132 \text{ eV} = \Gamma_1 - \Gamma_0$  and as indirect gap:  $0.334 \text{ eV} = L_1 - \Gamma_0$ . Moreover, analyzing the orbital-character of the band structure: we found that the eigenvectors corresponding to  $\Gamma_0$  and  $\Gamma_1$ , were mainly due to *p* and *s* states, respectively. Meanwhile, the eigenvectors at  $L_1$  were due to *s* and *s\** states. These results were analogous to those obtained for pure Ge, which indicated that the relative weights of the orbital contributions to the electronic properties of  $\text{Ge}_{1-x}\text{Sn}_x$  were weakly dependent of the Sn-content in the substitutional alloy.



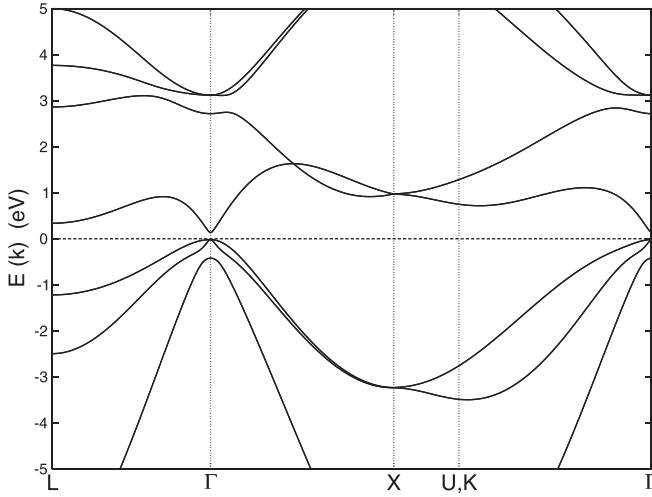


FIG. 4. The  $\text{Ge}_{0.78}\text{Sn}_{0.22}$  substitutional alloy: band structure  $E(\vec{k})$  obtained along the BZ paths of the face-centered cubic diamond lattice, between symmetry points:  $\Gamma = (0, 0, 0)$ ,  $L = (2\pi/a)(1/2, 1/2, 1/2)$ ,  $X = (2\pi/a)(1, 0, 0)$ ,  $U = (2\pi/a)(1, 1/4, 1/4)$ , and  $K = (2\pi/a)(3/4, 3/4, 0)$ , being  $a$  the lattice parameter. The parameters used for the present TB + VCA, as in Fig. 3.

### B. $\text{Ge}_{1-x}\text{Sn}_x$ : The TB + VCA results including $\alpha$ -Sn and $\beta$ -Sn, metallization transition

In Sec. III A, we showed that  $\text{Ge}_{1-x}\text{Sn}_x$  possesses an indirect fundamental gap at low Sn-concentrations and that, by increasing the Sn-concentration, the substitutional binary alloy undergoes a crossover from an indirect to a direct bandgap at  $x_c^I \sim 0.088$ . At higher Sn-concentrations, the non-substitutional  $\beta$ -Sn defects appear in the binary alloy, as predicted theoretically<sup>19,20</sup> and confirmed by experiments.<sup>21</sup> We will now show that the presence of  $\beta$ -Sn reduces the concentration range where  $\text{Ge}_{1-x}\text{Sn}_x$  possesses a direct gap, i.e., it reduces the critical concentration  $x_c^{II}$  at which the direct gap closes, corresponding to the metallization transition.

We analyzed the effect of both the substitutional and non-substitutional Sn defects on the electronic structure of  $\text{Ge}_{1-x}\text{Sn}_x$  employing the TB + VCA extension proposed in the present work, detailed in Section II.

To assess the effect of the  $\beta$ -Sn defects on the electronic structure, in particular, on the bandgaps, in Fig. 5(a), we plotted the TB + VCA band structure of  $\text{Ge}_{0.78}\text{Sn}_{0.22}$  along the  $L - \Gamma - X$  Brillouin zone path, for a fixed total Sn-concentration  $x = x_\alpha + x_\beta = 0.22$ , but different relative contents of the  $\alpha$ -Sn and non-substitutional  $\beta$ -Sn. It can be found that, when  $x_\beta$  increases, for example, from 0 to 0.035, the bandgap decreases: a progressive reduction of the direct gap at  $\Gamma$  upon increase of the  $\beta$ -Sn concentration was observed. In Fig. 5(b), we show the effect of  $\beta$ -Sn upon the DOS, for fixed total Sn-concentration  $x = 0.22$  and varying the relative  $\beta$ -Sn content in the alloy. The changes induced by increasing the  $\beta$ -Sn concentration on the density of states were less noticeable than those obtained in the band structure (see Fig. 5(a)). The progressive reduction of the gap confirmed that the presence of the non-substitutional  $\beta$ -Sn favours the metallization in  $\text{Ge}_{1-x}\text{Sn}_x$ .

In Fig. 6, we plotted the direct gap energy  $E_0$ , for the binary alloy with a fixed total Sn-concentration  $x = 0.22$  as a

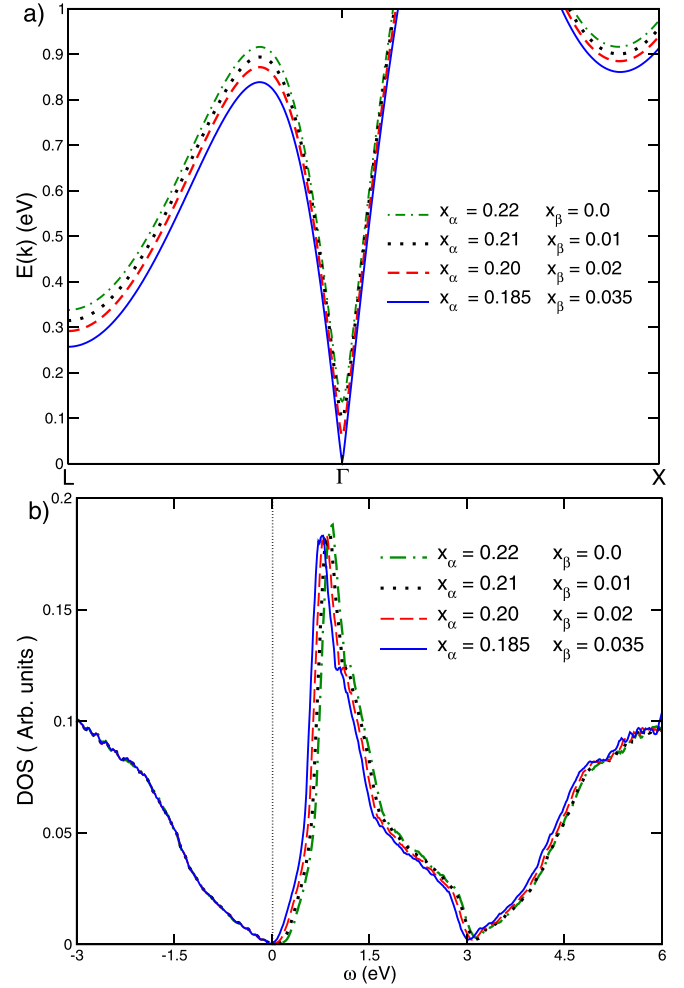


FIG. 5. (a) The  $\beta$ -Sn effect on the band structure of  $\text{Ge}_{0.78}\text{Sn}_{0.22}$ : the lowest conduction band along  $L - \Gamma - X$  path for different values  $x_\beta$  of  $\beta$ -Sn content, as indicated in the plot. (b) Effect of  $\beta$ -Sn on the DOS of  $\text{Ge}_{0.78}\text{Sn}_{0.22}$ : relative  $\beta$ -Sn similar to Fig. 6(a). The parameters used for the present TB + VCA extension, as in Fig. 3.

function of  $x_\beta$  (i.e.,  $x_\alpha = 0.22 - x_\beta$ ), for four different values of hopping  $t'$  between  $\beta$ -Sn and its Ge nearest-neighbours. A linear dependence of  $E_0$  as a function of  $x_\beta$  was obtained. The critical concentration  $x_c^{II}$  at which the direct gap closes, and the alloy becomes metallic, is strongly dependent on  $t'$  in our approach.

Analyzing the effect of the non-substitutional  $\beta$ -Sn on the total and partial densities of states, using our TB + VCA approach, we found that the relative weights of the orbital contributions to the electronic properties of  $\text{Ge}_{1-x}\text{Sn}_x$  were weakly dependent on the Sn-content.

Experimentally, the critical Sn-concentration  $x_c^{II}$  for the metallization transition in  $\text{Ge}_{1-x}\text{Sn}_x$  is yet unknown. As shown in Fig. 2, the gap measurements were reported at relatively low Sn-concentrations:  $x < 0.15$ .<sup>4,7,16,28,41,55</sup> More recently, the direct gap was determined in the homogeneous epitaxial layers of  $\text{Ge}_{1-x}\text{Sn}_x$  grown on the InP substrates<sup>12</sup> for  $0.15 < x < 0.27$ , from the photon absorption spectra measured with the Fourier transform infrared spectroscopy. In particular, for  $\text{Ge}_{0.73}\text{Sn}_{0.27}$ , Nakatsuka *et al.*<sup>12</sup> obtained a direct gap of  $\sim 0.25$  eV, so that the metallization of these epitaxial layers would occur at  $x > 0.27$ .



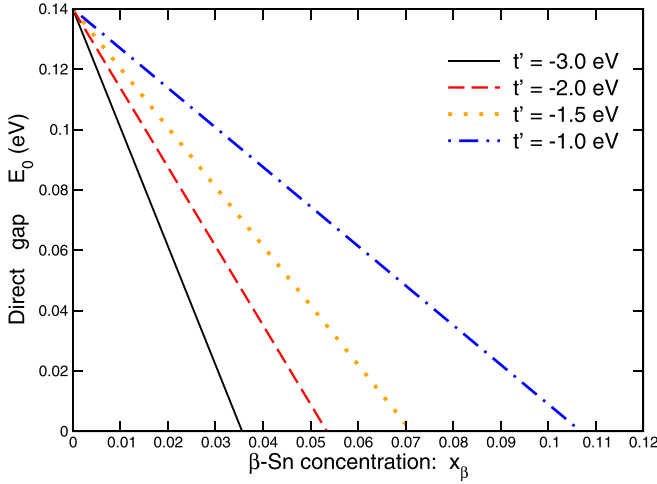


FIG. 6.  $t'$  dependence of the metallization transition for  $\text{Ge}_{0.78}\text{Sn}_{0.22}$ : energy value at  $\Gamma_0(E_0)$  as a function of  $x_\beta$ , for different values of  $t'$ . Other parameters used for the present TB + VCA extension, as in Fig. 3.

Additional measurements for higher Sn-concentrations would be required to locate the metallization transition in bulk  $\text{Ge}_{1-x}\text{Sn}_x$ . Extrapolating the experimental data fits, two predictions for  $x_c^{II}$  were obtained:  $x_c^{II} \sim 0.30$  by Atwater *et al.*,<sup>7</sup> and  $x_c^{II} \sim 0.37$  by D'Costa *et al.*<sup>4</sup>

On the other hand, Jenkins and Dow predicted  $x_c^{II} \sim 0.62$ <sup>33</sup> with their original TB + VCA approach for the substitutional  $\text{Ge}_{1-x}\text{Sn}_x$ . If we would consider only the substitutional  $\alpha$ -Sn to be present and use our present TB + VCA extension, we would predict for the transition from a direct gap to a metallic regime:  $x_c^{II} \sim 0.26$ , the same value which can be obtained if using the TB parameters for  $\alpha$ -Sn reported in Ref. 46.

In 2009, we proposed a statistical model for the formation of the  $\beta$ -Sn defects in  $\text{Ge}_{1-x}\text{Sn}_x$ ,<sup>19,20</sup> from which the relative concentrations of  $\beta$ -Sn (and  $\alpha$ -Sn) in the alloy can be obtained as a function of temperature and the total Sn-concentration  $x$ .

Using the statistical model<sup>19,20</sup> to determine  $x_\beta$  in  $\text{Ge}_{1-x}\text{Sn}_x$  (and from it:  $x_\alpha = x - x_\beta$ ), we can explore the dependence of the critical concentration for metallization  $x_c^{II}$  on the only free parameter ( $t'$ ) in our present approach. Furthermore, if  $x_c^{II}$  values were experimentally known, they might be used to tune the free parameter  $t'$ . In Figure 7, we addressed this issue, by plotting  $t'$  corresponding to the  $x_c^{II}$  values in the range from 0.22 to 0.5 for different temperatures  $T$ . Specifically, for  $T = 16^\circ\text{C}$ ,  $32^\circ\text{C}$ ,  $62^\circ\text{C}$ ,  $85^\circ\text{C}$ , and  $131^\circ\text{C}$ , while the relative contents  $x_\beta$  and  $x_\alpha$  are obtained from the statistical model.<sup>19,20</sup>

Figure 7 shows that, for  $0.22 \leq x_c^{II} < 0.26$ ,  $t'$  is negative and increases monotonically with an increasing  $x_c^{II}$ . On the other hand, for  $x_c^{II} \geq 0.26$ ,  $t'$  is positive. It can be noted that, all of these graphs in Fig. 7 intersect at  $x_c^{II} = 0.26$ , which corresponds to  $t' = 0$ , which in our model is equivalent to considering only the substitutional Sn to be present.

For instance, if we consider the temperature  $T = 16^\circ\text{C}$ , by adjusting  $t' \sim 1.0037$  eV, we would obtain a value  $x_c^{II} = 0.30$ , as suggested extrapolating the experiments of

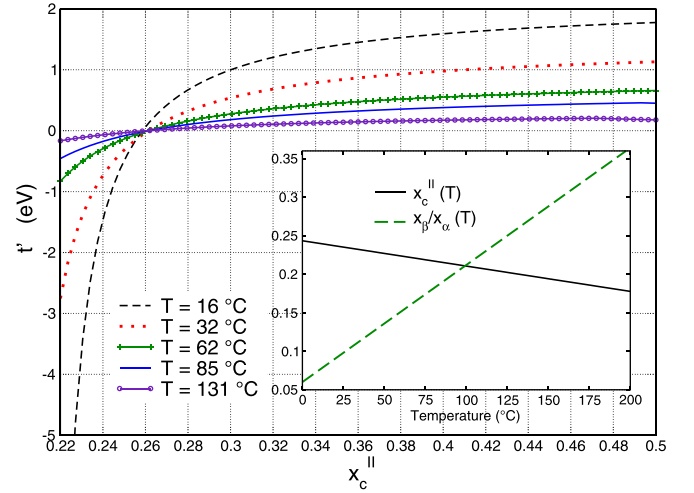


FIG. 7.  $t'$  hopping values as a function of the critical Sn concentration for metallization:  $x_c^{II}$ , at different temperatures. Inset: temperature dependence of the relative proportion of non-substitutional to substitutional Sn,  $x_\beta/x_\alpha$ , at  $x = x_c^{II}$  as obtained from the statistical model of Refs. 19 and 20; and, as a result, our prediction for the temperature dependence of the metallization transition:  $x_c^{II}(T)$ , for  $t' = -3$  eV.

Ref. 7, while, if we consider the same temperature but adjust  $t' \sim 1.4920$  eV, we would obtain a value  $x_c^{II} = 0.37$ , as suggested by extrapolating the experiments of Ref. 4.

The inset of Figure 7 depicts, for  $t' = -3$  eV, the temperature dependence obtained in our approach for the critical concentration for metallization,  $x_c^{II}$  (full line), and for the ratio between the non-substitutional  $\beta$ -Sn and the substitutional  $\alpha$ -Sn (dashed line) concentrations at  $x = x_c^{II}$  from Refs. 19 and 20. The inset reveals an increase in  $x_\beta/x_\alpha$  as a function of temperature, while a decrease in  $x_c^{II}$  as a function of temperature is observed. These results indicate that increasing the non-substitutional Sn content leads to a lower  $x_c^{II}$ , i.e., confirming that the presence of  $\beta$ -Sn favours metallization. It would be interesting to have this prediction confirmed by other theoretical approaches.

As we mentioned in the Introduction, the main interest for technological applications of  $\text{Ge}_{1-x}\text{Sn}_x$  is linked to its direct gap phase.<sup>1,4</sup> However, our results show that the concentration range ( $\Delta x = x_c^{II} - x_c^I$ ), in which  $\text{Ge}_{1-x}\text{Sn}_x$  possesses a direct fundamental gap would be reduced if the temperature of formation of the alloy is increased, since  $\beta$ -Sn might appear at lower Sn-concentrations. An important aspect in the fabrication of high-quality thin films using the molecular beam epitaxy is the growth-temperature.<sup>1,4,56,57</sup> Therefore, a detailed experimental study of the electronic properties of these alloys, including the second gap transition (metallization), could allow to determine the optimal growth conditions to control the proportion of  $\beta$ -Sn in  $\text{Ge}_{1-x}\text{Sn}_x$ .

#### IV. CONCLUSIONS

We have studied the effect of the  $\beta$ -Sn non-substitutional complex defects on the electronic structure of the  $\text{Ge}_{1-x}\text{Sn}_x$  binary alloy.

In order to include the non-substitutional complex defects in an electronic structure calculation, we presented

our extension of the method originally proposed by Jenkins and Dow for substitutional  $\text{Ge}_{1-x}\text{Sn}_x$ , using 20 tight-binding  $sp^3s^*$  orbitals for the group IV elements combined with the virtual crystal approximation. We included the complex non-substitutional  $\beta$ -Sn defects through the introduction of an effective substitutional two-site equivalent cluster for them, which we appropriately embedded in the lattice to calculate the electronic structure of the effective alloy purely in terms of the substitutional defects.

Our method allows to describe the two transitions of the fundamental gap of  $\text{Ge}_{1-x}\text{Sn}_x$  as a function of the total Sn concentration. In particular: (i) with our proposed extension for the tight-binding matrix, we could tune the critical Sn concentration  $x_c^I$  for the transition from an indirect to a direct gap, in agreement with the most recent experimental data. Our extension also improved the theoretical description of the direct gap experimental values for ternary  $\text{Ge}_{1-x-y}\text{Si}_x\text{Sn}_y$  alloys, as shown in the [Appendix](#). (ii) The metallization transition (closure of the direct gap) of  $\text{Ge}_{1-x}\text{Sn}_x$  at higher  $x = x_c^{II}$  can also be described, and we demonstrated the relevance of the non-substitutional  $\beta$ -Sn for the determination of  $x_c^{II}$ . In fact, if  $x_c^{II}$  would be measured, it could be used to determine the hopping parameter ( $t'$ ) between the  $\beta$ -Sn defects and the Ge matrix, the only free parameter of our model. (iii) We predict the effect of temperature on the metallization transition  $x_c^{II}(T)$  (not yet experimentally measured), resulting from the increase with temperature of the ratio  $x_\beta/x_\alpha$  between the concentrations of the non-substitutional to the substitutional Sn in Ge (which we obtain from our statistical model for  $\text{Ge}_{1-x}\text{Sn}_x$ ).

We believe that the physical properties of  $\text{Ge}_{1-x}\text{Sn}_x$  are strongly affected by the Sn complex defects in the Ge matrix, such as  $\beta$ -Sn among others,<sup>20</sup> and future experimental work would provide further support and increase the usefulness of the present approach. Furthermore, the general idea we proposed to include the non-substitutional complex defects in the electronic structure calculations, by determining effective substitutional equivalent clusters to replace them and solve the problem in terms of purely substitutional effective alloys, has a wide potential for applications in other systems.

## SUPPLEMENTARY MATERIAL

The [supplementary material](#) can be viewed for a comparison of the bandstructure of pure  $\alpha$ -Sn and the ideal substitutional alloy at  $x = 0.15, 0.30$ , employing different parametrizations.

## ACKNOWLEDGMENTS

C.I.V. and J.D.F. are Investigadores Científicos of CONICET (Argentina). J.D.Q.F. has a fellowship from CONICET. C.I.V. acknowledges support for this work from CONICET (PIP 0702) and ANPCyT (PICT'38357; PICT Redes'1776), and R.A.B. from CONACyT project 179616.

## APPENDIX: APPLICATION TO $\text{Ge}_{1-x-y}\text{Si}_x\text{Sn}_y$ TERNARY ALLOYS

In 2013, we reported a first calculation of the electronic structure of  $\text{Ge}_{1-x-y}\text{Si}_x\text{Sn}_y$  ternary alloys,<sup>58</sup> employing a

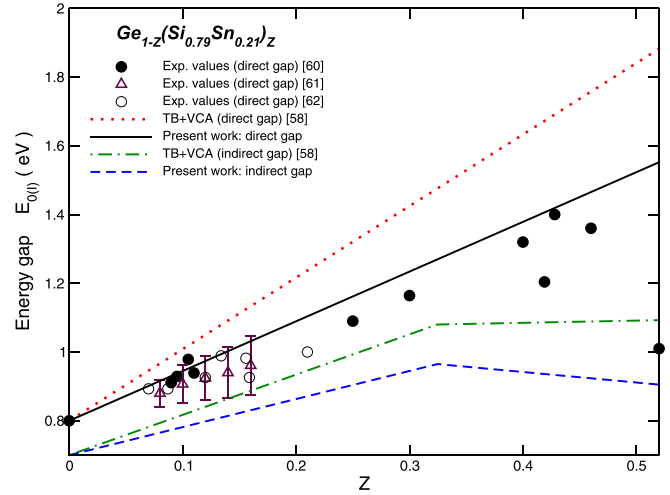


FIG. 8. The compositional dependence of the bandgap of  $\text{Ge}_{1-z}(\text{Si}_{0.79}\text{Sn}_{0.21})_z$  ternary alloys lattice-matched to Ge, obtained using the modified TB + VCA approach in the present work: direct gap (solid line) and indirect gap (dashed line). For comparison, we included our results from Ref. 58: direct gap (dotted line) and indirect gap (dashed-dotted line). Other data included for comparison correspond to experimental results for the direct gap from Refs. 60–62.

combined TB + VCA approximation method, which we developed as a direct extension to ternary substitutional alloys of the Jenkins and Dow approach<sup>33</sup> for binary substitutional  $\text{Ge}_{1-x}\text{Sn}_x$ . The same problem was later studied in Ref. 47 as well.

Our electronic structure results for ternary  $\text{Ge}_{1-x-y}\text{Si}_x\text{Sn}_y$  confirmed predictions and experimental indications that a 1 eV bandgap was attainable with these alloys, as required for the fourth layer planned to be added to present-day record-efficiency triple-junction solar cells, in order to further increase their efficiency for satellite applications.

It is interesting to apply the present TB + VCA parametrization for the substitutional alloy discussed in Section II B 1

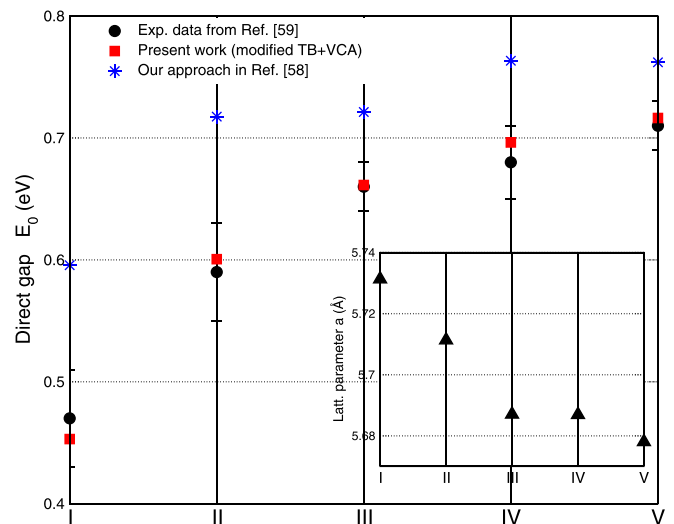


FIG. 9. A comparison of our theoretical results for the direct gap and lattice parameter with experimental data reported in Ref. 59, for the following ternary alloys: I:  $\text{Ge}_{0.864}\text{Sn}_{0.10}\text{Si}_{0.036}$ , II:  $\text{Ge}_{0.86}\text{Sn}_{0.082}\text{Si}_{0.058}$ , III:  $\text{Ge}_{0.94}\text{Sn}_{0.042}\text{Si}_{0.018}$ , IV:  $\text{Ge}_{0.916}\text{Sn}_{0.047}\text{Si}_{0.037}$ , and V:  $\text{Ge}_{0.947}\text{Sn}_{0.032}\text{Si}_{0.021}$ . Inset: lattice parameter for each of the ternary alloys I-V.

of the present work, in particular, the renormalized  $\alpha$ -Sn tight-binding parameters, as a starting point to recalculate the electronic structure of the ternary alloys and compare it with the results of our previous calculation.<sup>58</sup> We exhibit the comparison of the direct gap results as a function of composition in Figs. 8 and 9. In Fig. 8, one can see how the parametrized TB + VCA approach of the present work improves the description of the experimental compositional dependence of the direct gap with respect to our previous approach of Ref. 58 for a series of samples lattice-matched to Ge, while we also showed how the predicted indirect gap was slightly modified. In Fig. 9, we compared our present parametrized TB + VCA results for the direct gap with recent experimental results<sup>59</sup> for five ternary alloys with different lattice parameters (shown as inset): within the experimental error bars, the agreement was indeed very good for all samples, greatly improved with respect to the direct gap values predicted by the previous TB + VCA approach.<sup>58</sup>

- <sup>1</sup>M. R. Bauer, J. Taraci, J. Tolle, A. V. G. Chizmeshya, S. Zollmen *et al.*, *Appl. Phys. Lett.* **81**, 2992 (2002).
- <sup>2</sup>R. Hull and J. C. Bean, *Germanium Silicon: Physics and Materials, Semiconductors and Semimetals* (Academic, San Diego, 1999).
- <sup>3</sup>C. H. L. Goodman, *IEEE Proc., Part I: Solid-State Electron Devices Lett.* **129**, 189 (1982).
- <sup>4</sup>V. R. D'Costa, C. S. Cook, A. G. Birdwell, C. L. Littler, M. Canonico, S. Zollner, J. Kouvetakis, and J. Menendez, *Phys. Rev. B* **73**, 125207 (2006).
- <sup>5</sup>C. C. Yeo, B. J. Cho, F. Gao, S. J. Lee, M. H. Lee, C. Y. Yu, C. W. Liu, L. J. Tang, and T. W. Lee, *IEEE Electron Device Lett.* **26**, 761 (2005).
- <sup>6</sup>Y. J. Yang, W. S. Ho, C. F. Huang, S. T. Chang, and C. W. Liu, *Appl. Phys. Lett.* **91**, 102103 (2007).
- <sup>7</sup>G. He and H. A. Atwater, *Phys. Rev. Lett.* **79**, 1937 (1997); R. Ragan, K. S. Min, and H. A. Atwater, *Mater. Sci. Eng., B* **87**, 204 (2001).
- <sup>8</sup>J. D. Sau and M. L. Cohen, *Phys. Rev. B* **75**, 045208 (2007).
- <sup>9</sup>L. Lui, R. Liang, J. Wang, and J. Xu, *Appl. Phys. Express* **8**, 031301 (2015).
- <sup>10</sup>F. Gencarelli, D. Grandjean, Y. Shimura *et al.*, *J. Appl. Phys.* **117**, 095702 (2015).
- <sup>11</sup>M. R. Bauer, C. S. Cook, P. Aella *et al.*, *Appl. Phys. Lett.* **83**, 3489 (2003).
- <sup>12</sup>O. Nakatsuka, Y. Shimura, W. Takeuchi, N. Taoka, and S. Zaima, *Solid-State Electron.* **83**, 82 (2013).
- <sup>13</sup>L. Via, H. Höchst, and M. Cardona, *Phys. Rev. B* **31**, 958 (1985).
- <sup>14</sup>O. Gurdal, R. Desjardins, J. R. A. Carlsson, N. Taylor, H. H. Radamson, J. E. Sundgren, and J. E. Greene, *J. Appl. Phys.* **83**, 162 (1998).
- <sup>15</sup>H. Lin, R. Chen, Y. Huo, T. I. Kamins, and J. S. Harris, *Thin Solid Films* **520**, 3927 (2012).
- <sup>16</sup>R. Chen, H. Lin, Y. Huo *et al.*, *Appl. Phys. Lett.* **99**, 181125 (2011).
- <sup>17</sup>G. Grzybowski, R. T. Beeler, L. Jiang, D. J. Smith, J. Kouvetakis *et al.*, *Appl. Phys. Lett.* **101**, 072105 (2012).
- <sup>18</sup>W. Wegscheider, J. Olajos, U. Menezigar, U. Dondl, and G. Abstreiter, *J. Cryst. Growth* **123**, 75 (1992).
- <sup>19</sup>C. I. Ventura, J. D. Fuhr, and R. A. Barrio, *Physica B* **404**, 2830 (2009).
- <sup>20</sup>C. I. Ventura, J. D. Fuhr, and R. A. Barrio, *Phys. Rev. B* **79**, 155202 (2009).
- <sup>21</sup>S. Decoster, S. Cottenier, U. Wahl, J. G. Correia, and A. Vantomme, *Phys. Rev. B* **81**, 155204 (2010).
- <sup>22</sup>I. Chambouleyron, F. Marques, P. H. Dionisio, I. J. R. Baumvol, and R. A. Barrio, *J. Appl. Phys.* **66**, 2083 (1989).
- <sup>23</sup>J. D. Fuhr, C. I. Ventura, and R. A. Barrio, *J. Appl. Phys.* **114**, 193508 (2013), and references therein.
- <sup>24</sup>P. Capper and C. T. Elliott, *Infrared Detectors and Emitters: Materials and Devices*, 1st ed. (Kluwer Academic Publisher, New York, 2001).
- <sup>25</sup>E. Kasper, M. Oehme, T. Arguirov, J. Werner, M. Kittler, and J. Schulze, *Adv. Optoelectron.* **2012**, 916275 (2012).
- <sup>26</sup>W. Du, S. A. Ghetmiri, B. R. Conley, A. Mosleh *et al.*, *Appl. Phys. Lett.* **105**, 051104 (2014).
- <sup>27</sup>J. D. Gallagher, C. L. Senaratne, P. M. Wallace, J. Menéndez, and J. Kouvetakis, *Appl. Phys. Lett.* **107**, 123507 (2015).
- <sup>28</sup>H. P. Ladrón de Guevara, A. G. Rodríguez, H. Navarro-Contreras *et al.*, *Appl. Phys. Lett.* **91**, 161909 (2007).
- <sup>29</sup>M.-Y. Ryu, T. R. Harris, Y. K. Yeo, R. T. Beeler, and J. Kouvetakis, *Appl. Phys. Lett.* **102**, 171908 (2013).
- <sup>30</sup>W.-J. Yin, X.-G. Gong, and S.-H. Wei, *Phys. Rev. B* **78**, 161203 (2008).
- <sup>31</sup>J. D. Gallagher, C. L. Senaratne, J. Kouvetakis, and J. Menéndez, *Appl. Phys. Lett.* **105**, 142102 (2014); L. Jiang, J. D. Gallagher, C. L. Senaratne, T. Aoki, J. Mathews, J. Kouvetakis, and J. Menéndez, *Semicond. Sci. Technol.* **29**, 115028 (2014).
- <sup>32</sup>L. Jiang, C. Xu, J. D. Gallagher, R. Favaro, T. Aoki, J. Menéndez, and J. Kouvetakis, *Chem. Mater.* **26**, 2522 (2014).
- <sup>33</sup>D. W. Jenkins and J. D. Dow, *Phys. Rev. B* **36**, 7994 (1987).
- <sup>34</sup>K. E. Newman and J. D. Dow, *Phys. Rev. B* **30**, 1929 (1984).
- <sup>35</sup>D. J. Chadi, *Phys. Rev. B* **16**, 790 (1977).
- <sup>36</sup>D. J. Chadi and M. L. Cohen, *Phys. Status Solidi B* **68**, 405 (1975).
- <sup>37</sup>D. J. Chadi and M. L. Cohen, *Phys. Rev. B* **7**, 692 (1973).
- <sup>38</sup>R. A. Barrio, J. D. Querales Flores, J. D. Fuhr, and C. I. Ventura, *J. Supercond. Novel Magn.* **26**, 2213 (2013); J. D. Querales Flores, M.S. thesis, Instituto Balseiro, 2010.
- <sup>39</sup>L. Vegard, "Die Konstitution der Mischkristalle und die Raumfüllung der Atome," *Z. Phys.* **5**, 17–26 (1921).
- <sup>40</sup>P. Moontragoon, Z. Ikonik, and P. Harrison, *Semicond. Sci. Technol.* **22**, 742 (2007).
- <sup>41</sup>K. L. Low, Y. Yang, G. Han, W. Fan, and Y. C. Yeo, *J. Appl. Phys.* **112**, 103715 (2012).
- <sup>42</sup>Y. Chibane and M. Ferhat, *J. Appl. Phys.* **107**, 053512 (2010).
- <sup>43</sup>S. Gupta, B. Magyari-Köppe, Y. Nishi, and K. Saraswat, *J. Appl. Phys.* **113**, 073707 (2013).
- <sup>44</sup>C. Eckhardt, K. Hummer, and G. Kresse, *Phys. Rev. B* **89**, 165201 (2014).
- <sup>45</sup>R. Beeler, R. Roucka, A. V. G. Chizmeshya, J. Kouvetakis, and J. Menéndez, *Phys. Rev. B* **84**, 035204 (2011).
- <sup>46</sup>S. Küfner, J. Furthmüller *et al.*, *Phys. Rev. B* **87**, 235307 (2013).
- <sup>47</sup>A. Attiaoui and O. Moutanabbir, *J. Appl. Phys.* **116**, 063712 (2014).
- <sup>48</sup>P. Vogl, H. P. Hjalmarson, and J. D. Dow, *J. Phys. Chem. Solids* **44**, 365 (1983).
- <sup>49</sup>O. Madelung, *Semiconductors-Basic Data* (Springer, Berlin, 1996).
- <sup>50</sup>K. Koepf and H. Eschrig, *Phys. Rev. B* **59**, 1743 (1999); I. Opahle, K. Koepf, and H. Eschrig, *ibid.* **60**, 14035 (1999); K. Koepf, R. Velicky, R. Hayn, and H. Eschrig, *ibid.* **55**, 5717 (1997).
- <sup>51</sup>A. S. Carrico, R. J. Elliott, and R. A. Barrio, *Phys. Rev. B* **34**, 872 (1986).
- <sup>52</sup>J. Avendaño-López, F. L. Castillo-Alvarado, and R. A. Barrio, *Rev. Mex. Fis.* **40**, 750 (1994).
- <sup>53</sup>H. Lin, R. Chen, W. Lu, Y. Huo, T. I. Kamins *et al.*, *Appl. Phys. Lett.* **100**, 102109 (2012).
- <sup>54</sup>V. R. D'Costa, Y. Fang, J. Mathews *et al.*, *Semicond. Sci. Technol.* **24**, 115006 (2009).
- <sup>55</sup>H. Lin, R. Chen, Y. Huo *et al.*, *Appl. Phys. Lett.* **98**, 261917 (2011).
- <sup>56</sup>R. Roucka, J. Mathews, R. T. Beeler, J. Tolle, J. Kouvetakis *et al.*, *Appl. Phys. Lett.* **98**, 061109 (2011).
- <sup>57</sup>J. Mathews, R. T. Beeler, J. Tolle, C. Xu, R. Roucka *et al.*, *Appl. Phys. Lett.* **97**, 221912 (2010).
- <sup>58</sup>C. I. Ventura, J. D. Querales Flores, J. D. Fuhr, and R. A. Barrio, *Prog. Photovoltaics: Res. Appl.* **23**, 112 (2015).
- <sup>59</sup>C. Xu, L. Jiang, J. Kouvetakis, and J. Menéndez, *Appl. Phys. Lett.* **103**, 072111 (2013).
- <sup>60</sup>V. R. D'Costa, Y. Y. Fang, J. Kouvetakis, and J. Menéndez, *Phys. Rev. Lett.* **102**, 107403 (2009).
- <sup>61</sup>R. T. Beeler, C. Xu, D. J. Smith, G. Grzybowski, J. Menéndez, J. Kouvetakis *et al.*, *Appl. Phys. Lett.* **101**, 221111 (2012).
- <sup>62</sup>C. Xu, R. T. Beeler, G. J. Grzybowski, A. V. G. Chizmeshya *et al.*, *J. Am. Chem. Soc.* **134**, 20756 (2012).